IEEE Access
Multidisciplinary | Rapid Review | Open Access Journal

Received January 5, 2018, accepted February 7, 2018, date of publication February 27, 2018, date of current version March 16, 2018.

Digital Object Identifier 10.1109/ACCESS.2018.2809658

Peak-to-Average Power Ratio of Multicarrier Faster-Than-Nyquist Signals: Distribution, Optimization and Reduction

AIJUN LIU, (Member, IEEE), SIMING PENG, (Student Member, IEEE), LI SONG, XIAOHU LIANG, KE WANG, AND QINGSHUANG ZHANG

Department of Satellite Communications, College of Communications Engineering, PLA University of Science and Technology, Nanjing 210007, China

Corresponding author: Siming Peng (lgdxpsm@gmail.com)

ABSTRACT Multicarrier faster-than-Nyquist (MFTN) is a spectral efficient transmission scheme for future communication systems. However, as one of the most important drawbacks of multicarrier transmission systems, the peak-to-average power ratio (PAPR) of MFTN signals is still not clear yet. In this paper, we investigate the PAPR of MFTN signals for nonlinear satellite communication systems. First of all, the PAPR distribution of MFTN signals under various practical situations is evaluated, and we show that the PAPR of MFTN signals is closely related to the number of subcarriers, the shaping pulse, and the time–frequency packing factors. Moreover, different from conventional Nyquist multicarrier signals, certain time–frequency packing in MFTN will however, improve the PAPR performance. Then, the PAPR of MFTN signals under the given spectral efficiency is considered. By jointly optimizing the time–frequency spacing to minimize the PAPR, we show that the MFTN combined with low-order modulation could be more energy efficient than the corresponding Nyquist high-order modulation signals. Finally, we investigate the PAPR reduction for MFTN signals. Specifically, a selective mapping-based alternative-signal scheme, which mainly intended for the conventional Nyquist multicarrier signals, is extended to the MFTN signaling system. It is shown that the PAPR reduction performance of the considered scheme is robust to the time–frequency packing, and even approaches the conventional orthogonal frequency-division multiplexing system. Our numerical results validate that besides the high spectral efficiency, the MFTN may be also an energy efficient transmission scheme for next-generation satellite communication systems.

INDEX TERMS Multicarrier transmission, faster-than-Nyquist, time-frequency packing, peak-to-average power ratio, selective mapping, satellite communications.

I. INTRODUCTION

In this bandwidth scarce and energy hungry world, the spectral and energy efficiency have become important considerations in designing practical communication systems [1], [2]. For the former target, it can be efficiently solved by the multicarrier faster-than-Nyquist (MFTN) signaling. The MFTN mainly relies on time-frequency packing of conventional Nyquist multicarrier transmission systems, such as orthogonal frequency division multiplexing (OFDM) or filter-bank multicarrier (FBMC). By reducing the time interval between adjacent symbols and packing the frequency spacing (or user bandwidth) between adjacent subcarriers, the spectral efficiency could be substantially improved with respect to the conventional Nyquist case. It was shown in [3] and [4] that the spectral efficiency of MFTN could be improved 100% more than the Nyquist signaling systems under the same time-frequency resources at the same bit energy and error rate. Due to this reason, the MFTN technique has drawn wide interests in future satellite and terrestrial mobile (5G) as well as optical communication systems [5]–[9].

The concept of single carrier FTN can be dated back to 1975s, which was firstly proposed by Mazo in [10]. In this study, he pointed out that the binary sinc pulses could be sent faster without loss in asymptotic error probability. This he called FTN since the pulses appear faster than allowed by Nyquist's limit for orthogonal pulses. Since the sinc pulse is not applicable for practical implementation, the FTN based on root raised cosine (RRC) pulse has been investigated in 2003 in [11], and it was shown that by exploiting the excess bandwidth of RRC pulse, the Mazo limit, i.e., the minimum

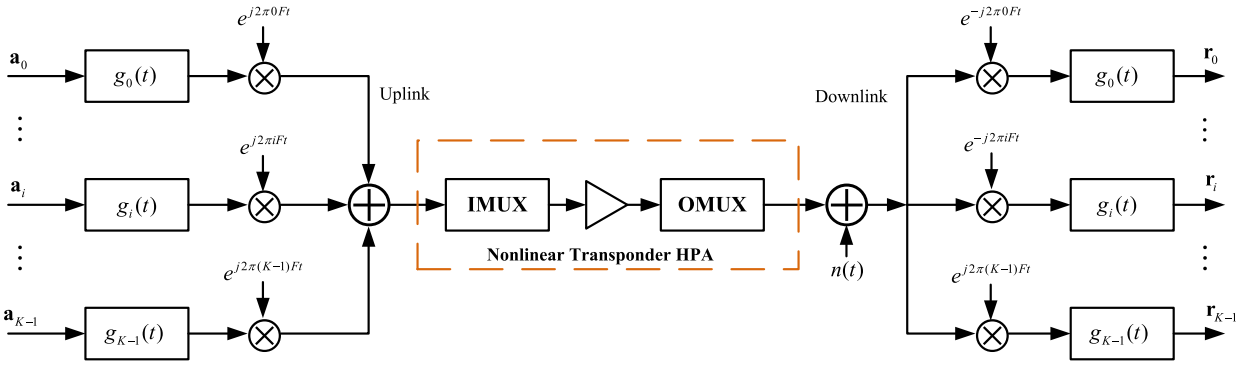

FIGURE 1. Satellite system model with K carriers amplified simultaneously by a single onboard HPA.

time packing factor above which the Euclidean distance could be kept as the Nyquist case, is better than the sinc pulse. However, it was not until 2005 that the concept of FTN has been extended to the frequency domain, i.e., multicarrier FTN [12]. By reducing the frequency spacing between adjacent subcarriers, it was shown that the two dimensional Mazo limit of MFTN could be further improved than the single carrier case.

On the other hand, the energy efficiency is also of paramount importance, especially in the resource-limited satellite communication systems [13], [14]. To ensure that the amplification is power efficient, the high power amplifiers (HPAs) are often driven close to the saturation point. However, it is known that the efficiency of HPA is directly related to the peak-to-average power ratio (PAPR) of the input signal, and these HPAs will lead to nonlinear distortion. For example, high order modulations, such as 16 or 32 amplitude and phase shift keying (APSK) are often used to increase spectral efficiency in the Digital Video Broadcasting-Satellite-Second Generation (DVB-S2) system [15]. However, these modulation schemes are sensitive to the nonlinear distortions introduced by the onboard HPA. Moreover, the nonlinear effects of the HPA become even more prominent when multiple carriers are amplified using a single HPA [16]–[18]. Such a situation arises when different carriers share the same onboard HPA due to power/mass and flexibility requirements. A schematic diagram of the multicarrier satellite system in this case is shown in Fig. 1. Additionally, the use of multiple carriers in satellite communication leads to high PAPR, which requires an increase in the back-off used for power amplification, thereby leading to a loss in power efficiency.

Unfortunately, current attentions about MFTN mainly focus on the Euclidean distance (or Mazo limit), spectral efficiency as well as practical detection schemes [19]–[23], and the works concerning the PAPR of MFTN signals are still not enough yet in the literatures. For example, the soft input and soft output (SISO) frequency domain equalization (FDE) has been proposed for the detection of MFTN signals in [20]. By exploiting the principle of iterative Turbo equalization, the ISI and ICI free BER performance could be approximately approached with low complexity. In [21], a maximum signal-to-interference ratio (SIR) time-frequency packing scheme has been proposed for MFTN signaling system, and it showed that the time-frequency packing could obtain better spectral efficiency than conventional time packing or frequency packing scheme. Moreover, by optimizing the lattice structure of MFTN signals, a hexagonal lattice-based MFTN signaling system has been proposed in [22], and it showed that the Mazo limit could be further improved by the hexagonal MFTN. On the other hand, in [24]–[26], the PAPR of single carrier FTN signals has been investigated, and it was shown that the time packing will have an impact on the ultimate PAPR distribution of FTN signals. Recently, a partial transmit sequence (PTS) PAPR reduction scheme which making use of the discrete Fourier transform (DFT)-based implementation of the MFTN transmitter has been proposed in [27], however, due to the adjacent subcarriers in MFTN are not orthogonal to each other anymore, the overhead of side-information is extremely high and the resulting PAPR reduction is also not so attractive. Furthermore, although it was predicted in [3] and [23] that the MFTN may have higher PAPR than Nyquist signals, no comprehensive investigation has ever been conducted to validate this argument.

On the other hand, the PAPR problem has been widely investigated in conventional Nyquist multicarrier transmission systems, and many PAPR reduction techniques have been also proposed in the literatures [28] and [29]. Specifically, due to the shaping pulse utilized in FBMC is longer than the symbol period, it was pointed out in [30] and [31] that the PAPR reduction schemes which mainly intended for OFDM signals could not be directly employed in FBMC transmission systems (note that the FBMC can be viewed as a special case of MFTN without time-frequency packing). Hence, many modified PAPR reduction schemes by incorporating the overlapping between adjacent data blocks have been tailored for FBMC signaling systems. However, since the time-frequency packing degrades the orthogonality between adjacent carriers and pulses, it is thus unclear whether the PAPR reduction

schemes intended for FBMC signals could be utilized to reduce the PAPR of MFTN signals or a complete redesign of the PAPR reduction scheme for MFTN signals is required.

Regarding these issues, we investigate the PAPR of MFTN signals in this paper. Firstly, we make a comprehensive evaluation of the PAPR distribution in MFTN signaling system under various practical situations. It is shown that besides the number of subcarriers and excess bandwidth of the shaping pulse, the time-frequency packing factors will also make a contribution to the ultimate PAPR distribution. Moreover, we demonstrate that the PAPR of MFTN signals could be refined under proper time and/or frequency packing. Based on this observation, we then jointly optimize the time-frequency spacing under the given spectral efficiency so that the PAPR of MFTN signals could be minimized. In this regard, we also compare the PAPR of low order modulated MFTN signals with its high order modulated counterparts under the same spectral efficiency, and reveal that the MFTN signaling system with proper time-frequency spacing could be more energy efficient than conventional Nyquist signaling systems. Finally, a selective mapping (SLM)-based alternative-signal (AS) scheme which mainly intended for FBMC signals is extended to MFTN signaling system. Our numerous simulation results validate that the PAPR reduction performance of the adopted scheme is robust to the time-frequency packing, and could even approach the OFDM system under the similar conditions.

The reminder of this paper is organized as follows. In Section II, the preliminaries in terms of the MFTN signaling in satellite communication system and the PAPR problem are introduced briefly. The PAPR distribution of MFTN signals under different situations is evaluated in Section III, following which, the PAPR of MFTN signals is optimized in Section IV. In Section V, the AS algorithm is utilized to reduce the PAPR of MFTN signals, and finally, the conclusion is summarized in Section VI.

II. PRELIMINARIES

The MFTN and Nyquist symbols over time-frequency grid are shown in Fig. 2. We consider a forward link of a transparent satellite system where synchronous users employ the same linear modulation format, shaping pulse $g(t)$ and symbol interval T, and access the channel according to a frequency division multiplexing scheme and share the same transponder HPA. We assume that the modulated uncorrected and identical distributed information symbols $\{a_{l,k}\}$ (being l the time index and k the carrier/user index) belong to a given zero-mean $\mathcal{M}$-th order complex constellation, the transmitted linear modulation signal is given by

$$s(t) = \sqrt{E_s} \sum_{l} \sum_{k} a_{l,k} g(t - l\tau T) e^{j2\pi k \upsilon F t} \tag{1}$$

where E_s is the mean energy per symbol and is used to normalize the average power of each user. T is the Nyquist time interval and F is the minimum orthogonal frequency spacing between adjacent channels, respectively.

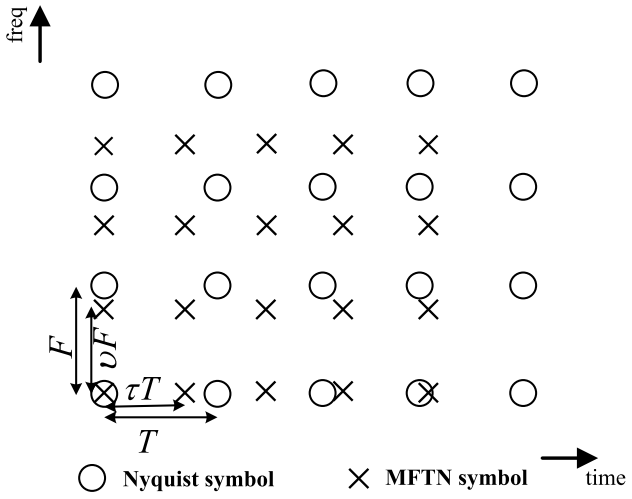

FIGURE 2. MFTN and Nyquist symbols over time-frequency grid.

In DVB-S2 standard, the base pulse is an RRC pulse with roll-off factor β (equal to 0.2, 0.3 or 0.35 depending on the service requirements). In case of pulses employed in DVB-S2, we have $F = (1 + \beta)/T$. Moreover, τ is the time interval packing factor and υ is the frequency spacing (or user bandwidth) packing factor, respectively. We remark that in MFTN signaling system, one more degree of freedom of system optimization is the bandwidth F of the shaping pulse $g(t)$. Hence, even the bandwidths may be kept fixed for input and output multiplexing (IMUX and OMUX) filters used in the nonlinear satellite channel, the frequency packing can be equivalently implemented by increasing the pulse bandwidth F [5]. We define $T_\Delta = \tau T$ and $F_\Delta = \upsilon F$ as the packed time spacing and frequency spacing, respectively. For conventional Nyquist signaling system, we have $\tau \cdot \upsilon = 1$, while for MFTN signaling system, $\tau \cdot \upsilon < 1$. Without loss of generality, T_Δ and F_Δ will be normalized to some reference values T and F. We will also assume $T = 1$ as in [3] and [4] throughout the following parts of this paper.

In general, the PAPR is a convenient parameter to measure the sensitivity to non-linear amplification of the transmission schemes having a non-constant envelope. It is shown in (1) that the *symbol rate* of MFTN is $1/(\tau T)$, and thus the length of each MFTN symbol is equal to LT, $L \in \mathbb{N}_+$, where LT is the length of the shaping pulse, the length of the MFTN signal $s(t)$ is thus $LT + (M - 1)\tau T$, and M is the number of transmitted MFTN symbols. Similar as general FBMC system [30], [31], we firstly divide the MFTN signals into $\lfloor L/\tau \rfloor + M - 1$ intervals equally with the time duration τT. Hence, the PAPR in each interval is defined as

$$PAPR_p \triangleq \frac{\max\limits_{p\tau T \le t < (p+1)\tau T} |s(t)|^2}{\mathrm{E}[|s(t)|^2]},\ p = 0, 1, \ldots, \lfloor L/\tau \rfloor + M - 2 \tag{2}$$

where $\mathrm{E}[\cdot]$ denotes the expectation operation.

Generally, the PAPR performance can be evaluated by the complementary cumulative distribution function (CCDF) and

which is defined as the probability that the PAPR exceeds a given level $PAPR_0 > 0$, i.e.,

$$CCDF = \Pr(PAPR > PAPR_0) \tag{3}$$

III. PAPR DISTRIBUTION OF MFTN SIGNALS

Assume that the Nyquist discrete time symbol period is N and the number of subcarriers is K. We will also assume T is a multiple of the sampling interval T_c, and the sampling rate that is used for discretizing all the signals is $1/T_c = KF$. By defining $s[n] = s(nT_c)$, the discrete time samples of the MFTN signal (1) can be expressed as

$$s[n] = \sqrt{E_s} \sum_{l=0}^{M-1} \sum_{k=0}^{K-1} a_{l,k} g[n - l\tau N] e^{j2\pi k \upsilon n/K} \tag{4}$$

In general, we are more interested in the PAPR of continuous-time MFTN signals, even we may directly deal with the discrete time samples. Hence, to better approximate the PAPR of continuous-time MFTN signals, the MFTN signal samples are obtained by J times oversampling. Similar to conventional Nyquist multicarrier signals, the J times oversampled time-domain samples vector $\mathbf{a}_l$ can be obtained by $(J-1)K$ zeros-padding for the l-th data block, i.e.,

$$\mathbf{a}_l = [a_{l,0}, \ldots, a_{l,K-1}, \underbrace{0, \ldots, 0}_{(J-1)K}]^T \tag{5}$$

where $[\cdot]^T$ is the matrix/vector transpose operation.

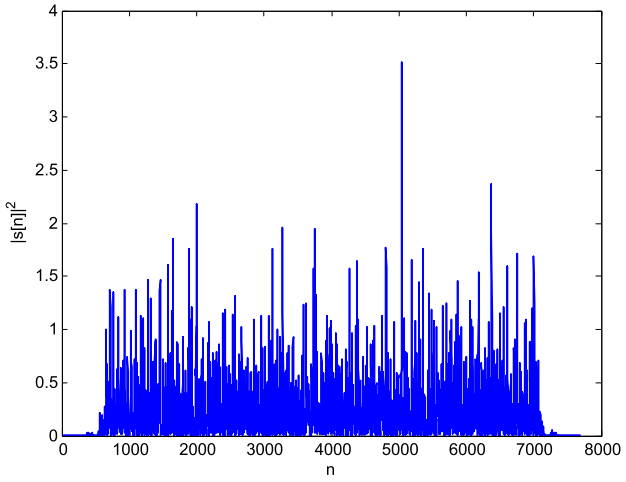

FIGURE 3. Peak power of the MFTN signals. In this figure, the number of subcarriers is $K = 60$, and the RRC pulse with roll-off factor $\beta = 0.3$ is employed. Moreover, the time-frequency spacing considered here is $T_\Delta = 0.9, F_\Delta = 0.9$.

As an example, Fig. 3 shows the peak power $|s[n]|^2$ under different time instants, where the number of subcarriers is $K = 60$, RRC pulse with $\beta = 0.3$ and $T_\Delta = 0.9, F_\Delta = 0.9$ have been employed. Obviously, the maximum instantaneous signal power may be far larger than its average power. Hence, the PAPR problem must be carefully considered in MFTN signaling system.

According to (4), the PAPR computed from the J-times oversampled time domain MFTN signal samples can be thus defined as

$$PAPR_p = \frac{\max\limits_{p\tau JN \le n < (p+1)\tau JN} |s[n]|^2}{\mathrm{E}[|s[n]|^2]} \tag{6}$$

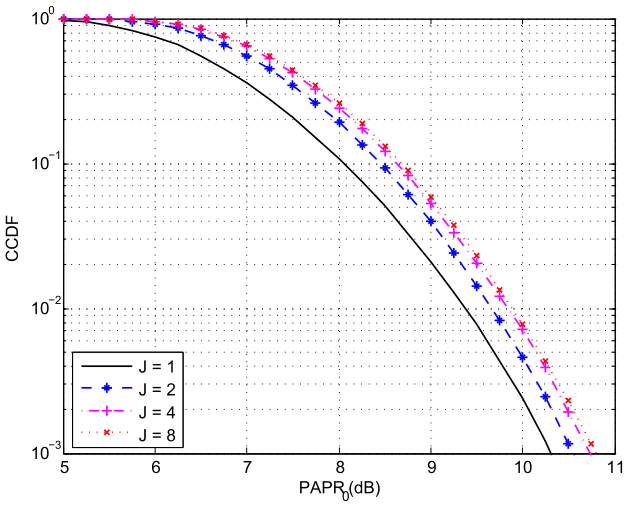

FIGURE 4. PAPR distribution of MFTN signals under different oversampling factors. In this figure, the number of subcarriers is $K = 60$, and the RRC pulse with roll-off factor $\beta = 0.3$ is employed. Moreover, the time-frequency spacing considered here is $T_\Delta = 1, F_\Delta = 1$.

Fig. 4 shows the PAPR distribution of MFTN signals under different oversampling factors, where the number of subcarriers is $K = 60$, QPSK modulation (unless otherwise specified, QPSK will be the default modulation format in this section) is employed and $J = 1, 2, 4, 8$ have been taken into consideration. Moreover, the time-frequency spacing is $T_\Delta = 1$, $F_\Delta = 1$, and the roll-off factor of RRC pulse is $\beta = 0.3$. From this figure, we can see that the oversampling factor has an impact on the ultimate PAPR distribution of MFTN signals, and when $J \ge 4$, it will be sufficient to obtain accurate PAPR results. Based on this observation, the oversampling factor $J = 4$ will be employed throughout the following parts of this paper.

In [33] and [34], the analytical expressions to accurately describe the PAPR distribution of OFDM signals have been presented, and which are considered to be greatly simplified the system design process. However, things will be changed and similar works will be more complex in MFTN signaling system. The reasons can be briefly organized as follows. Firstly, different from OFDM signals mainly based on the rectangular pulse where the date blocks in different symbol intervals are mutually independent, the shaping pulse in MFTN is longer than the symbol period. Hence, the data blocks in adjacent time intervals are overlapped with each other. Due to this reason, the closed-form of the bounds regarding the PAPR distribution for FBMC signals is still not available yet. Secondly, due to the time-frequency packing introduced in MFTN signaling system, the subcarriers and

adjacent shaping pulses will be not orthogonal to each other anymore, and which further complicates the derivation of the accurate PAPR distribution of MFTN signals (it should be noted that in this regard, the PAPR of MFTN signals will be jointly determined by the modulation format, the number of subcarriers K, the time-frequency packing factors τ, υ as well as the adopted shaping pulse $g(t)$). Hence, for the sake of simplicity, we will mainly rely on the numerical analysis in this paper.

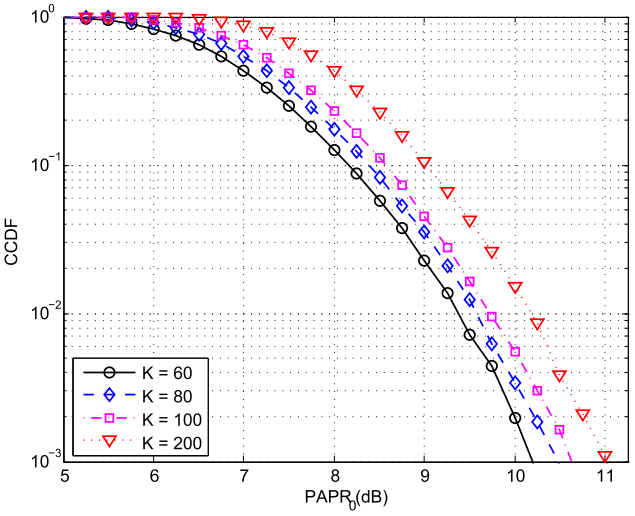

FIGURE 5. PAPR distribution of MFTN signals under different number of subcarriers K. In this figure, the time-frequency spacing are chosen to be $T_\Delta = 0.8$, $F_\Delta = 0.8$. Moreover, the oversampling factor is $J = 4$ and roll-off factor $\beta = 0.3$ have been employed.

Fig. 5 presents the PAPR distribution of MFTN signals under different number of subcarriers, where $K = 60, 80, 100, 200$ and $T_\Delta = 0.8, F_\Delta = 0.8$ have been considered in the simulations. As we can see from this figure that similar as general multicarrier signals, the PAPR will be deteriorated with the increase of the number of subcarriers K. Hence, more attentions should be paid to the MFTN signals especially for the case of large number of subcarriers.

Then, we turn to focus on evaluating the effect of time-frequency packing on the PAPR distribution of MFTN signals. In the numerical experiments, the number of subcarriers is $N = 60$, and the RRC pulse with $\beta = 0.3$ has been considered. Firstly, we present the PAPR distribution of MFTN signals under different frequency spacing in Fig. 6, where we fix the time spacing to $T_\Delta = 1$ and the frequency spacing $F_\Delta = 1, 0.8, 0.6, 0.5$ have been utilized.[1] Interesting, we can see that with the reduction of the frequency packing factor υ or the frequency spacing F_Δ, the PAPR performance will be however, improved. For example, the PAPR of MFTN signals under $F_\Delta = 0.5$ is approximately 0.5dB better than $F_\Delta = 1$. Furthermore, the PAPR distribution of MFTN

[1] We point out that owing to the potential high signal detection complexity of the receiver, the time-frequency packing factor will be in general not too small in MFTN signaling system.

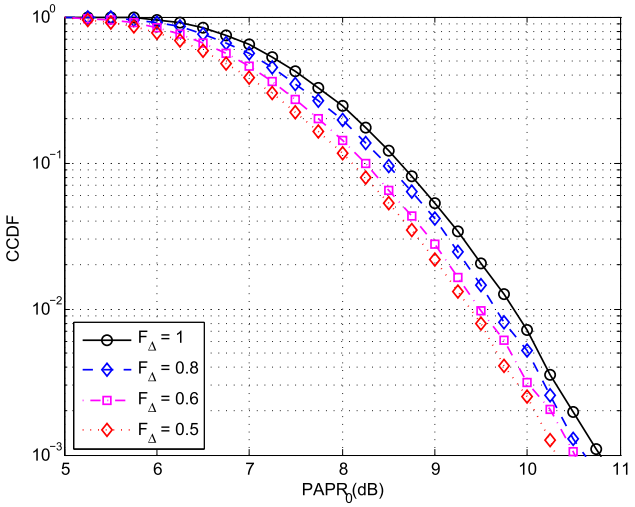

FIGURE 6. PAPR distribution of MFTN signals under different frequency spacing. In this figure, the number of subcarriers is $K = 60$, and the RRC pulse with roll-off factor $\beta = 0.3$ is employed. Moreover, the time spacing is fixed to $T_\Delta = 1$.

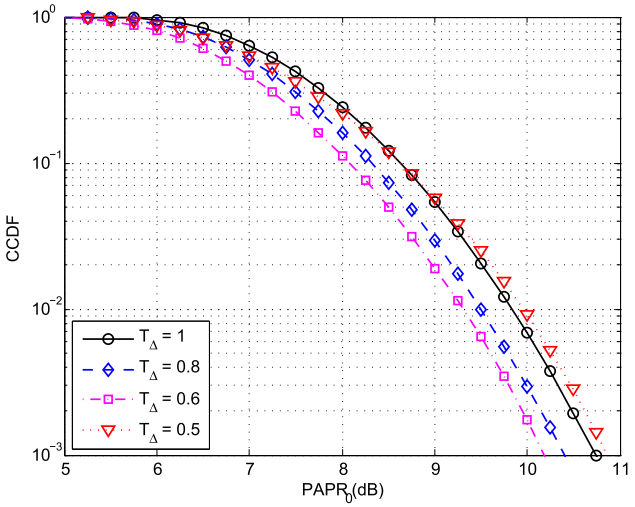

FIGURE 7. PAPR distribution of MFTN signals under different time spacing. In this figure, the number of subcarriers is $K = 60$, and the RRC pulse with roll-off factor $\beta = 0.3$ is employed. Moreover, the frequency spacing is fixed to $F_\Delta = 1$.

signals under frequency spacing $F_\Delta = 1$ and different time spacing is shown in Fig. 7. As we can see from this figure that similar as frequency packing, certain time packing will also improve the PAPR distribution of MFTN signals. However, when the time packing factor is small enough, e.g., $T_\Delta \leq 0.5$, the PAPR distribution will be deteriorated than other cases. The reason for this phenomenon is due to that according to the central limit theory, the summation of the independent symbols in K uncorrelated subcarriers will in general result in the worst PAPR distribution (in this regard, the ultimate signal will be quite approach the Gaussian distribution when K is large enough). However, due to the time-frequency packing and pulse shaping employed in MFTN signaling system, the symbols in different data blocks will be *not*

independent to each other anymore. Consequently, the PAPR distribution could be refined in certain extent. We point out that similar phenomenon can be also found in the PAPR distribution of spectral efficient frequency division multiplexing (SEFDM) signals in [35], where only frequency packing has been employed. Indeed, the time-frequency packing and pulse shaping could be viewed as a kind of precoding scheme, and the PAPR of MFTN signals can be thus improved under certain situations.

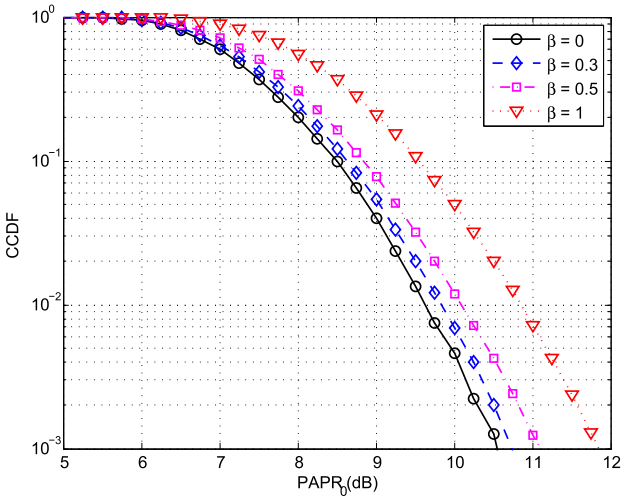

FIGURE 8. PAPR distribution of MFTN signals under different roll-off factors of the shaping pulse. In this figure, the number of subcarriers is $K = 60$, and the RRC pulse with roll-off factor $\beta = 0.3$ is employed. Moreover, the time-frequency spacing are chosen to be $T_\Delta = 1, F_\Delta = 1$.

Finally, we present the PAPR distribution of MFTN signals based on RRC pulse with different roll-off factors β in Fig. 8, where $T_\Delta = 1, F_\Delta = 1$ and $K = 60$ have been employed. It is known that the excess bandwidth of RRC pulse plays an important role in determining the Mazo limit performance of FTN signaling system, and in general, the Mazo limit will be improved with the increase of the excess bandwidth of the RRC pulse. From Fig. 8, we can find that the roll-off factor also has an impact on the PAPR distribution of MFTN signals. Moreover, the PAPR of MFTN signals under $\beta = 1$ is 1.4dB higher than $\beta = 0$ under the same conditions, which also demonstrates that with the increase of the roll-off factor β or equivalently, the excess bandwidth, the PAPR performance will be deteriorated as a result.

IV. PAPR OPTIMIZATION OF MFTN SIGNALS

In Section III, we have shown that the time-frequency packing factor or time-frequency spacing has an impact on the PAPR distribution of MFTN signals. Naturally, two interesting problems arise, i.e., for the given target spectral efficiency η, what is the optimal time-frequency spacing so that the PAPR could be minimized? and how is the PAPR performance of MFTN combined with low order modulation compared with the higher order modulation under the same spectral efficiency? In this section, we will try to solve these problems.

Base on above discussions, the optimization problem can be formulated as follow[2]

$$\min_{T_\Delta, F_\Delta} \max_{pT_\Delta \le t < (p+1)T_\Delta} |s(t)|^2$$
$$\text{Subject to. } \eta = \log_2|\mathcal{M}| / (T_\Delta F_\Delta) \tag{7}$$

We point out that due to the complex MFTN signal structure (pulse shaping and time-frequency packing), an elegant theoretical derivation to solve (7) is an impractical task. Hence, for the sake of simplicity, we will mainly resort to the numerical analysis in this section. Moreover, in the numerical experiments, four modulation schemes in DVB-S2 standard, i.e., QPSK, 8PSK, 16APSK and 32APSK are considered, and the length of the shaping pulse is $6T$ and the RRC pulse with roll-off factor $\beta = 0.3$ has been utilized. Also, even the time-frequency packing may introduce serious intersymbol interference (ISI) and intercarrier interference (ICI), we will assume that the target spectral efficiency could be obtained by proper equalization schemes at the receiver.

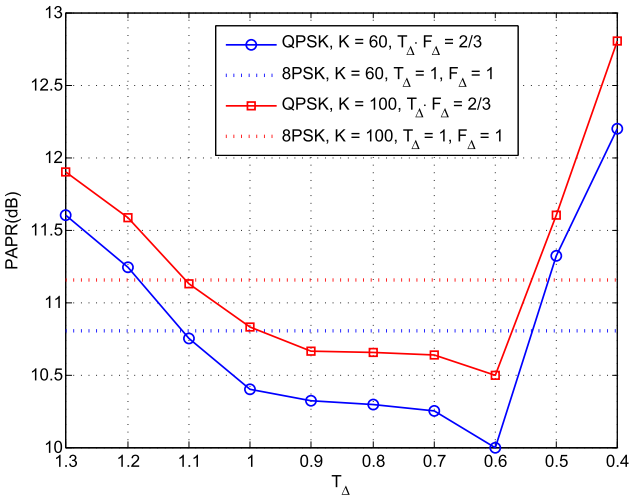

FIGURE 9. PAPR of MFTN signaling system under the target spectral efficiency $\eta = 3$ bits/s/Hz. In this figure, the oversampling factor is $J = 4$ and the RRC pulse with roll-off factor $\beta = 0.3$ is employed. Moreover, the PAPR under $CCDF = 10^{-3}$ is extracted.

Firstly, we give the PAPR performance of MFTN signaling system with QPSK modulation under the target spectral efficiency $\eta = 3$ bits/s/Hz in Fig. 9. To this end, the time-frequency spacing is restricted to be $T_\Delta \cdot F_\Delta = 2/3$. As a reference, the PAPR performance with 8PSK modulation under $T_\Delta = 1, F_\Delta = 1$ is also shown for comparison, and the PAPR under $CCDF = 10^{-3}$ is extracted. We remark that although not shown here, the PAPR of Nyquist multicarrier signals, i.e., $T_\Delta = 1, F_\Delta = 1.3$, is quite approach the MFTN signals at $T_\Delta = 1, F_\Delta = 1$ for the four modulation schemes (no more than 0.2dB). From this figure, we can find that similar as Fig. 7, when $T_\Delta \ge 0.6$, the PAPR of MFTN signals will be

[2]For the sake of simplicity, we only consider the uncoded case. However, similar conclusion also holds true for the coded case, since the interleaver concatenated to the encoder will also obtain the independent information data.

reduced with the reduction of time spacing T_Δ. While on the other hand, the PAPR will be increased if the time spacing T_Δ is further reduced (note that the frequency spacing will be increased accordingly). Hence, there is an optimal time-frequency spacing which could result in the lowest PAPR performance. Moreover, it is seen that the PAPR performance of the optimized MFTN with QPSK modulation could be improved as much as 0.8dB than the conventional Nyquist signals under 8PSK modulation.

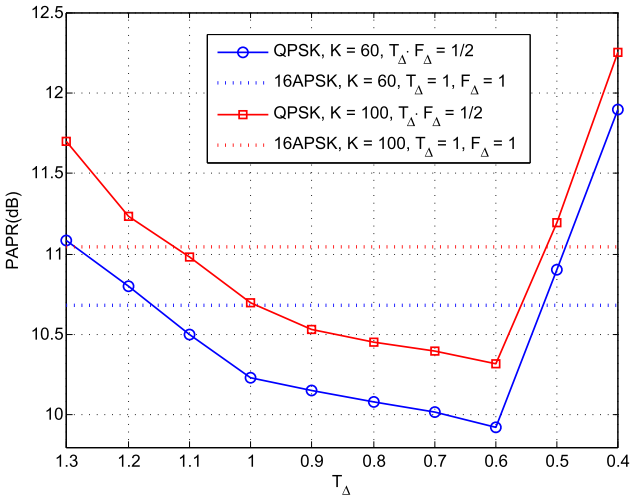

FIGURE 10. PAPR of MFTN signaling system under the target spectral efficiency $\eta = 4$ bits/s/Hz. In this figure, the oversampling factor is $J = 4$ and the RRC pulse with roll-off factor $\beta = 0.3$ is employed. Moreover, the PAPR under $CCDF = 10^{-3}$ is extracted.

To further validate the practical benefit of MFTN signaling system, the PAPR performance of MFTN signals under the target spectral efficiency $\eta = 4$ bits/s/Hz is plotted in Fig. 10. Similarly, the PAPR based on 16APSK modulation under $T_\Delta = 1, F_\Delta = 1$ has been presented as a reference. It is seen that there is also an optimal time-frequency spacing which could minimize the PAPR of MFTN signals under the given spectral efficiency, and the PAPR of MFTN signals with QPSK modulation under $T_\Delta = 0.6$ is approximately 0.9dB better than the 16APSK modulation for both the cases of $K = 60$ and $K = 100$. Hence, in practical applications, $T_\Delta \in [0.6, 1]$ may be a good choice to obtain improved energy efficiency.

Finally, the PAPR performance of MFTN signaling system under target spectral efficiency $\eta = 5$ bits/s/Hz is presented in Fig. 11. In this regard, the PAPR based on 32APSK modulation under $T_\Delta = 1, F_\Delta = 1$ has been presented as a reference. Specifically, three other modulation schemes, i.e., QPSK, 8PSK, 16APSK, have been also considered. The number of subcarriers is fixed to $K = 100$. From this figure, we can find that the MFTN combined with QPSK modulation and proper time-frequency packing could obtain 0.9dB PAPR improvement than the 32APSK modulation, and more than 0.3dB improvement than the 8PSK and 16APSK modulations under the same spectral efficiency.

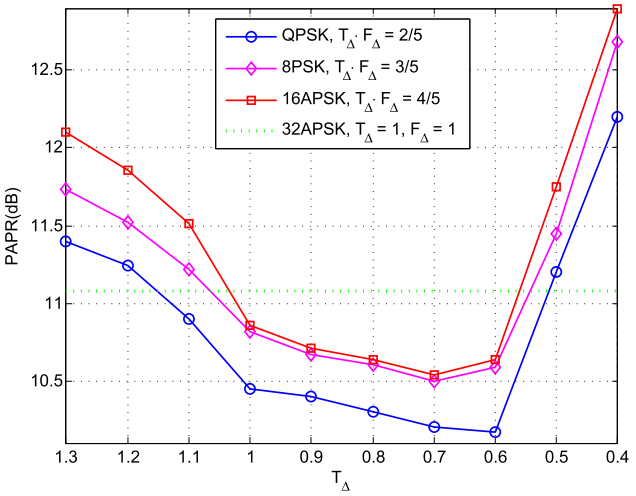

FIGURE 11. PAPR of MFTN signaling system under the target spectral efficiency $\eta = 5$ bits/s/Hz. In this figure, the number of subcarriers is $K = 100$. The oversampling factor is $J = 4$ and the RRC pulse with roll-off factor $\beta = 0.3$ is employed. Moreover, the PAPR under $CCDF = 10^{-3}$ is extracted.

Hence, all in all, from the simulation results presented above, we may conclude that the low order modulation coupled with MFTN and optimized time-frequency spacing could be more energy efficient than conventional Nyquist high order modulation systems under the same spectral efficiency.

V. PAPR REDUCTION OF MFTN SIGNALS

From above analysis and numerical results, we can find that even the time-frequency spacing optimization could obtain refined PAPR performance, there is still a high PAPR exists among MFTN signals. Hence, in practical applications, an efficient PAPR reduction scheme may be also expected.

As we have mentioned before, some novel PAPR reduction schemes by making use of the specific MFTN signal structure could be designed. However, it is known that the PAPR problem has been widely investigated in conventional OFDM and FBMC signaling systems, and many PAPR reduction schemes have been also proposed in the literatures. Hence, in this section, we will mainly focus on exploiting the existing PAPR reduction scheme proposed for conventional Nyquist multicarrier signals, and evaluating its practical performance utilized in MFTN signaling system.

Before proceeding, we would like to give a brief discussion on the available PAPR reduction schemes. According to [29], the PAPR reduction schemes for multicarrier signals could be mainly classified into two categories. The first one is the pre-distortion scheme such as clipping and filtering [36] and companding transform [37]. The second one is the distortionless scheme such as precoding [38], selective mapping (SLM) [39], partial transmit sequence (PTS) [40] and so on. Due to the serious ISI and ICI induced by time-frequency packing in MFTN signaling system, the predistortion schemes will be ruled out and we will therefore focus

on the distortionless PAPR reduction schemes. On the other hand, owing to the similarities between MFTN and FBMC signals (such as the shaping pulse), a natural choice is to employ the PAPR reduction scheme intended for FBMC signals to MFTN signaling system. Based on these observations, the sequential alternative-signal (AS) method based on SLM proposed in [41] will be extended to reduce the PAPR of MFTN signals in this section.[3]

A. PAPR REDUCTION OF MFTN SIGNALS WITH AS

According to Fig. 1, the transmitted MFTN signal $s(t)$ can be obtained in several steps. Firstly, the MFTN symbols on the l-th data block passed through the prototype filter can be expressed as

$$x_k^l(t) = a_{l,k} g(t - l\tau T) \tag{8}$$

Then, $x_k^l(t), k = 0, 1, \ldots, K-1$ are modulated with K subcarriers to obtain

$$s_k^l(t) = x_k^l(t) e^{j2\pi k \upsilon F t}, \quad k = 0, 1, \ldots, K-1 \tag{9}$$

Next, $s_k^l(t)$ on all of the K subcarriers are added up together to obtain the l-th MFTN symbol $s^l(t)$ as

$$s^l(t) = \sum_{k=0}^{K-1} s_k^l(t), \quad l\tau T \le t < (l + L - 1)\tau T \tag{10}$$

Finally, the desired MFTN signal $s(t)$ is obtained by summing over the M MFTN symbols, i.e.,

$$s(t) = \sum_{l=0}^{M-1} s^l(t), \quad 0 \le t < (\lfloor L/\tau \rfloor + M - 1)\tau T \tag{11}$$

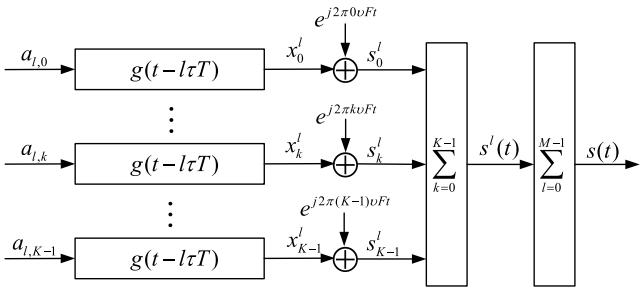

FIGURE 12. MFTN transmitter.

The above procedures are also depicted in Fig. 12. According to the principle of SLM, the AS reduces the PAPR by optimally choosing one phase rotation vector from a given set for each MFTN symbol. Over different MFTN symbols, the phase rotation vectors might be different. Denotes the set of candidate phase rotation vectors as

$$\mathbf{B} = \{\mathbf{b}_0, \mathbf{b}_1, \ldots, \mathbf{b}_{U-1}\} \tag{12}$$

[3]We choose the SLM-based AS scheme because of the SLM scheme has been also widely employed to reduce the PAPR of conventional OFDM signals. Moreover, the AS proposed in [41] exploits the overlapping of FBMC symbols between adjacent data blocks, and the complexity of this scheme is also acceptable for practical communication systems.

where U is the size of $\mathbf{B}$, and $\mathbf{b}^u, 0 \le u < U-1$, is the u-th phase rotation vector, which is defined as

$$\mathbf{b}^u = [b_0^u, b_1^u, \ldots, b_{K-1}^u]^T \tag{13}$$

with $b_k^u = e^{j2\pi i/W}, i = 0, 1, \ldots, W-1$. For the sake of simplicity, we adopt $W = 2$, and $\mathbf{b}^{l,u} = [b_0^{l,u}, b_1^{l,u}, \ldots, b_{K-1}^{l,u}]^T$ as the phase rotation vector used by the l-th MFTN symbol $s^l(t)$. Without loss of generality, $\mathbf{B}$ is assumed to be known at both the transmitter and receiver.

Due to the overlapped signal structure, the main idea of the AS algorithm adopted here is based on the sequential optimization procedure. In the l-th data block, by taking into account the previous MFTN symbols, i.e., $s^0(t), s^1(t), \ldots, s^{l-1}(t)$, we reduce the peak power of $s^l(t)$. More details are formulated as follows.

For the zero-th symbol, we multiply $s^0(t)$ by different phase rotation vectors and choose the one with the minimum peak power, which is denoted as $\hat{s}^0(t)$. Then, $\hat{s}^0(t)$ is sent to the first symbol to solve the following optimization problem, i.e.,

$$\min_{\mathbf{b}^{1,u}} \max_{2\tau T \le t < (2+\Gamma)\tau T} \left| \hat{s}^0(t) + \sum_{k=0}^{K-1} s_k^1(t) b_k^{1,u} \right|^2$$
$$\text{Subject to. } \mathbf{b}^{1,u} \in \mathbf{B} \tag{14}$$

where Γ is a parameter that may affect the PAPR reduction performance, and according to [41], $L/2+1 \le \Gamma \le L$ will be adopted. It should be also noted that we adopt the peak power as the design metric in this section. Moreover, given the finite dimensionality of $\mathbf{B}$, exhaustive search will be adopted here to identify the optimal $\mathbf{b}^{l,u}$. Similar to conventional SLM, for each MFTN symbol $s^m(t)$, the complexity of searching the optimal phase rotation vector $\mathbf{b}^{l,u}$ is on the order of $\mathcal{O}(U)$, and the overall complexity of searching the M optimal phase rotation vectors is on the order of $\mathcal{O}(UM)$. Furthermore, since $\log_2(U)$ bits are needed for each MFTN signal $s^m(t)$, $m = 0, 1, \ldots, M-1$, the overhead of side information for all the M symbols is thus $M\log_2(U)$ bits.

Following (14), the optimal phase rotation vector is denoted as $\mathbf{b}^{1,u^*}$, and the newly generated symbol is thus

$$\hat{s}^1(t) = \sum_{k=0}^{K-1} s_k^1(t) b_k^{1,u^*} \tag{15}$$

Then, $\hat{s}^1(t)$ and $\hat{s}^0(t)$ are both sent to the second block to calculate the new symbol $\hat{s}^2(t)$. We repeat the above procedure until the $(M-1)$-th block.

The general procedure of AS algorithm for the l-th MFTN symbol, $l = 1, 2, \ldots, M-1$, can be expressed as follows

$$\min_{\mathbf{b}^{l,u}} \max_{(l+1)\tau T \le t < (l+\Gamma)\tau T} \left| \sum_{i=0}^{l-1} \hat{s}^i(t) + \sum_{k=0}^{K-1} s_k^l(t) b_k^{l,u} \right|^2$$
$$\text{Subject to. } \mathbf{b}^{l,u} \in \mathbf{B} \tag{16}$$

B. SIMULATION RESULTS

In this subsection, we perform the numerical simulations to evaluate the PAPR reduction performance based on the AS algorithm described above. In the simulations, the number of subcarriers/users is fixed to $K = 60$, and the RRC pulse with length $6T$ and roll-off factor $\beta = 0.3$ as well as QPSK modulation has been employed. The oversampling factor is chosen to be $J = 4$, $\Gamma = 5$, and 10^4 simulations are performed to average the results.

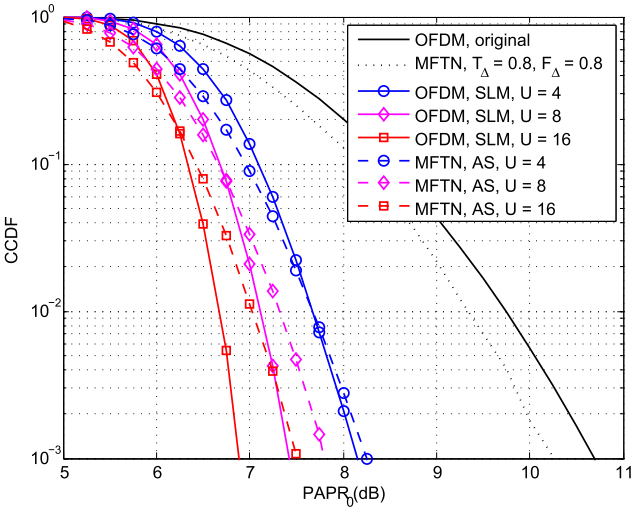

FIGURE 13. PAPR reduction performance of OFDM and MFTN signals under different number of phase rotation vectors U. In this figure, the time-frequency spacing for MFTN signaling system is fixed to $T_\Delta = 0.8, F_\Delta = 0.8$.

Fig. 13 presents the PAPR reduction performance of MFTN signals by exploiting the AS algorithm, where the number of candidate phase rotation vectors $U = 4, 8, 16$ have been employed, and the time-frequency spacing is chosen to be $T_\Delta = 0.8, F_\Delta = 0.8$. Moreover, the PAPR distribution of OFDM signals as well as the PAPR reduction performance based on SLM is also shown for comparison. From this figure, we can find that the PAPR distribution of original MFTN signals is 0.5dB better than the OFDM signals. When $U = 4$, the OFDM and MFTN signals could achieve similar PAPR performance, and with the increase of U, better PAPR reduction performance could be obtained for both OFDM and MFTN signals. Moreover, even the PAPR performance of AS algorithm for MFTN signals is worse than SLM for OFDM under $U = 8$ and $U = 16$, the gap between them is no more than 0.7dB.[4]

[4]It should be noted that due to the overlapped signal structure, the AS algorithm utilized here adopts the suboptimal solution, while for SLM, we used the optimal phase rotation vector for per OFDM symbol. Hence, there is a slight degradation of the PAPR reduction performance for MFTN signaling system with respect to the case of OFDM (i.e., the PAPR reduction achieved by SLM for OFDM can be viewed as a low bound for AS algorithm to MFTN signaling system). Moreover, we remark that the complexity to obtain the optimal phase rotation vectors by jointly optimizing all the M MFTN symbols is on the order of $\mathcal{O}(U^M)$, which makes the exhaustive search method impractical. Hence, the computational complexity of the adopted scheme could be greatly reduced than the optimal scheme.

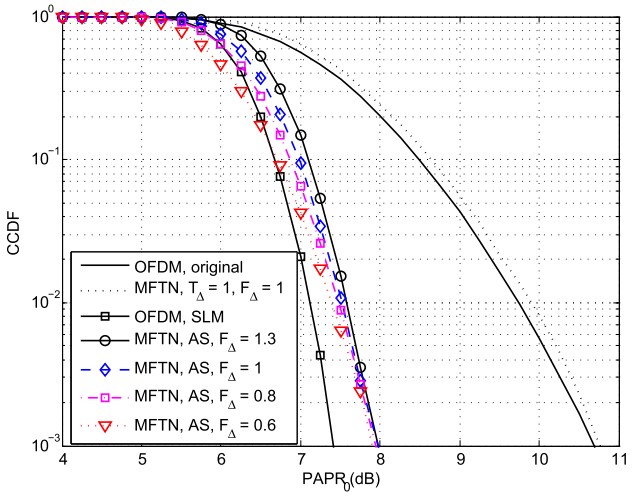

FIGURE 14. PAPR reduction performance of MFTN signals under different frequency spacing. In this figure, $T_\Delta = 1$, $U = 8$, $K = 100$ have been employed.

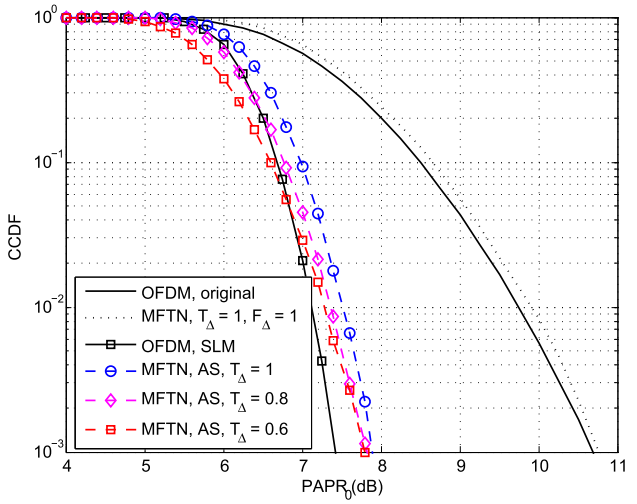

FIGURE 15. PAPR reduction performance of MFTN signals under different time spacing. In this figure, $F_\Delta = 1$, $U = 8$, $K = 100$ have been employed.

In order to further validate the potential impacts of time-frequency packing with respect to the PAPR reduction performance for MFTN signals, Fig. 14 gives the PAPR reduction performance of MFTN signals under frequency spacing $F_\Delta = 1.3, 1, 0.8, 0.6$, where the time spacing $T_\Delta = 1$ and $U = 8$ have been employed. As a benchmark, the PAPR distribution of original MFTN signals under $T_\Delta = 1, F_\Delta = 1$ has been also shown in this figure. It is interesting to see that the PAPR reduction performance of MFTN signals is robust to the frequency packing under the given parameter sets.[5] Similar phenomenon can be also found in Fig. 15, where the frequency spacing is fixed to $F_\Delta = 1$ and the PAPR reduction performance under time spacing $T_\Delta = 1, 0.8, 0.6$ have been evaluated.

[5]Indeed, the AS or SLM could be also treated as a kind of precoding scheme. In this regard, the effect of time-frequency packing will be alleviated compared with the AS/SLM on the ultimate PAPR reduction performance.

Hence, from the simulation results presented above, we may conclude that the PAPR of MFTN signals could be substantially reduced by exploiting the AS algorithm, and the time-frequency packing also only has a slight impact on the ultimate PAPR reduction performance.

VI. CONCLUSION

In this paper, we investigated the PAPR of spectral efficient MFTN signals, where a comprehensive evaluation of the PAPR performance has still not been conducted yet. In this regard, the PAPR distribution of MFTN signals under various practical situations has been analyzed firstly, and we showed that certain time-frequency packing could refine the PAPR of MFTN signals. Moreover, we optimized the time-frequency spacing values of MFTN signaling system under the given spectral efficiency so that the ultimate PAPR could be minimized. Our numerical results demonstrated that the MFTN signaling system could obtain lower PAPR than conventional Nyquist transmission systems. Finally, a state-of-the-art PAPR reduction scheme which mainly intended for Nyquist multicarrier signals has been extended to MFTN signaling system. It was shown that there is only a slight effect of the time-frequency packing on the ultimate PAPR reduction performance. Hence, the MFTN technique may be a better choice than conventional Nyquist multicarrier transmission schemes from the point of view of spectral and energy efficiency for future satellite and terrestrial mobile communication systems.

REFERENCES

[1] J. B. Anderson, F. Rusek, and V. Öwall, "Faster-than-Nyquist signaling," *Proc. IEEE*, vol. 101, no. 8, pp. 1817–1830, Aug. 2013.
[2] G. Wunder, R. F. H. Fischer, H. Boche, S. Litsyn, and J.-S. No, "The PAPR problem in OFDM transmission: New directions for a long-lasting problem," *IEEE Signal. Process. Mag.*, vol. 30, no. 6, pp. 130–144, Nov. 2013.
[3] F. Rusek and J. B. Anderson, "Multistream faster than Nyquist signaling," *IEEE Trans. Commun.*, vol. 57, no. 5, pp. 1329–1340, May 2009.
[4] A. Barbieri, D. Fertonani, and G. Colavolpe, "Time-frequency packing for linear modulations: Spectral efficiency and practical detection schemes," *IEEE Trans. Commun.*, vol. 57, no. 10, pp. 2951–2959, Oct. 2009.
[5] A. Piemontese, A. Modenini, G. Colavolpe, and N. S. Alagha, "Improving the spectral efficiency of nonlinear satellite systems through time-frequency packing and advanced receiver processing," *IEEE Trans. Commun.*, vol. 61, no. 8, pp. 3404–3412, Aug. 2013.
[6] T. Delamotte and G. Bauch, "Receiver design for GEO satellite systems using MIMO and time-frequency packing," in *Proc. Int. OFDM Workshop*, Essen, Germany, 2014, pp. 9–16.
[7] P. Banelli, S. Buzzi, G. Colavolpe, A. Modenini, F. Rusek, and A. Ugolini, "Modulation formats and waveforms for 5G networks: Who will be the heir of OFDM?" *IEEE Commun. Mag.*, vol. 31, no. 6, pp. 80–93, Nov. 2014.
[8] J. G. Andrews *et al.*, "What will 5G be?" *IEEE J. Sel. Areas Commun.*, vol. 32, no. 6, pp. 1065–1082, Jun. 2014.
[9] G. Colavolpe and T. Foggi, "Time-frequency packing for high-capacity coherent optical links," *IEEE Trans. Commun.*, vol. 62, no. 8, pp. 2986–2995, Aug. 2014.
[10] J. E. Mazo, "Faster-than-Nyquist signaling," *Bell Syst. Tech. J.*, vol. 54, no. 8, pp. 1451–1462, 1975.
[11] A. D. Liveris and C. N. Georghiades, "Exploiting faster-than-Nyquist signaling," *IEEE Trans. Commun.*, vol. 51, no. 9, pp. 1502–1511, Sep. 2003.
[12] F. Rusek and J. B. Anderson, "The two dimensional Mazo limit," in *Proc. ISIT*, Adelaide, SA, USA, Sep. 2005, pp. 970–974.
[13] S. Buzzi, C.-L. I, T. E. Klein, H. V. Poor, C. Yang, and A. Zappone, "A survey of energy-efficient techniques for 5G networks and challenges ahead," *IEEE J. Sel. Areas Commun.*, vol. 34, no. 4, pp. 697–709, Apr. 2016.
[14] L. M. Correia *et al.*, "Challenges and enabling technologies for energy aware mobile radio networks," *IEEE Commun. Mag.*, vol. 48, no. 11, pp. 66–72, Nov. 2010.
[15] E. Casini, R. De Gaudenzi, and A. Ginesi, "DVB-S2 modem algorithms design and performance over typical satellite channels," *Int. J. Satellite Commun. Netw.*, vol. 22, no. 3, pp. 281–318, Jun. 2004.
[16] B. F. Beidas, "Intermodulation distortion in multicarrier satellite systems: Analysis and turbo Volterra equalization," *IEEE Trans. Commun.*, vol. 59, no. 6, pp. 1580–1590, Jun. 2011.
[17] E. Zenteno, R. Piazza, B. S. M. R. Rao, D. Rönnow, and B. Ottersten, "Low complexity predistortion and equalization in nonlinear multicarrier satellite communications," *EURASIP J. Adv. Signal Process.*, vol. 30, pp. 1–15, Mar. 2015.
[18] H. W. Kim, K. Kang, B. J. Ku, S. Kim, and D. I. Chang, "SAT-OFDM: A satellite radio interface for the IMT-advanced system," *Int. J. Satellite Commun. Network.*, vol. 33, no. 4, pp. 295–314, Apr. 2015.
[19] J. Fan, S. Guo, X. Zhou, Y. Ren, G. Ye Li, and X. Chen, "Faster-than-Nyquist signaling: An overview," *IEEE Access*, vol. 5, pp. 1925–1940, 2017.
[20] S. Peng, A. Liu, H. Fang, K. Wang, and X. Liang, "Turbo frequency domain equalization and detection for multicarrier faster-than-Nyquist signaling," in *Proc. Wireless Commun. Netw. Conf. (WCNC)*, Mar. 2017, pp. 1–6.
[21] S. Peng, A. Liu, X. Tong, and K. Wang, "On max-SIR time–frequency packing for multicarrier faster-than-Nyquist signaling," *IEEE Commun. Lett.*, vol. 21, no. 10, pp. 2142–2145, Oct. 2017.
[22] S. Peng, A. Liu, X. Pan, and H. Wang, "Hexagonal multicarrier faster-than-Nyquist signaling," *IEEE Access*, vol. 5, pp. 3332–3339, Mar. 2017.
[23] F. Schaich and T. Wild, "A reduced complexity receiver for multi-carrier faster-than-Nyquist signaling," in *Proc. IEEE Globecom*, Dec. 2013, pp. 235–240.
[24] C. Le, M. Schellmann, M. Fuhrwerk, and J. Peissig, "On the practical benefits of faster-than-Nyquist signaling," in *Proc. Int Conf. Adv. Technol.*, Oct. 2015, pp. 208–213.
[25] J.-A. Lucciardi, N. Thomas, M.-L. Boucheret, C. Poulliat, and G. Mesnager, "Trade-off between spectral efficiency increase and PAPR reduction when using FTN signaling: Impact of non linearities," in *Proc. Int Conf. Commun. (ICC)*, May 2016, pp. 1–7.
[26] T. Delamotte, A. Knopp, and G. Bauch, "Faster-than-Nyquist signaling for satellite communications: A PAPR analysis," in *Proc. Int ITG Conf. Syst. Commun. Coding (SCC)*, Feb. 2017, pp. 1–6.
[27] S. Peng, A. Liu, K. Wang, and X. Liang, "PAPR reduction of multicarrier faster-than-Nyquist signals with partial transmit sequence," *IEEE Access*, vol. 5, pp. 24931–24937, Dec. 2017.
[28] Y. Rahmatallah and S. Mohan, "Peak-to-average power ratio reduction in OFDM systems: A survey and taxonomy," *IEEE Commun Surveys Tuts.*, vol. 15, no. 4, pp. 1567–1592, 4th Quart., 2014.
[29] T. Jiang and Y. Wu, "An overview: Peak-to-average power ratio reduction techniques for OFDM signals," *IEEE Trans. Broadcast.*, vol. 54, no. 2, pp. 257–268, Jun. 2008.
[30] D. Qu, S. Lu, and T. Jiang, "Multi-block joint optimization for the peak-to-average power ratio reduction of FBMC-OQAM signals," *IEEE Trans. Signal Process.*, vol. 61, no. 7, pp. 1605–1613, Apr. 2013.
[31] C. Ye, Z. Li, T. Jiang, C. Ni, and Q. Qi, "PAPR reduction of OQAM-OFDM signals using segmental PTS scheme with low complexity," *IEEE Trans. Broadcast.*, vol. 60, no. 1, pp. 141–147, Mar. 2014.
[32] S. Peng, A. Liu, X. Liu, K. Wang, and X. Liang, "MMSE turbo equalization and detection for multicarrier faster-than-Nyquist signaling," *IEEE Trans. Veh. Technol.*, to be published.
[33] H. Ochiai and H. Imai, "On the distribution of the peak-to-average power ratio in OFDM signals," *IEEE Trans. Commun.*, vol. 49, no. 2, pp. 282–289, Feb. 2001.
[34] T. Jiang, M. Guizani, H.-H. Chen, W. Xiang, and Y. Wu, "Derivation of PAPR distribution for OFDM wireless systems based on extreme value theory," *IEEE Trans. Wireless Commun.*, vol. 7, no. 4, pp. 1298–1305, Apr. 2008.
[35] S. Isam and I. Darwazeh, "Peak to average power ratio reduction in spectrally efficient FDM systems," in *Proc. 18th Int. Conf. Telecommun.*, May 2011, pp. 363–368.

[36] H. Ochiai and H. Imai, "Performance of the deliberate clipping with adaptive symbol selection for strictly band-limited OFDM systems," *IEEE J. Sel. Areas Commun.*, vol. 18, no. 11, pp. 2270–2277, Nov. 2000.
[37] S. Peng and Z. Yuan, "A novel criterion for designing of nonlinear companding functions for peak-to-average power ratio reduction in multicarrier transmission systems," *Wireless Netw.*, vol. 24, no. 2, pp. 581–595, Feb. 2016.
[38] S. B. Slimane, "Reducing the peak-to-average power ratio of OFDM signals through precoding," *IEEE Trans. Veh. Technol.*, vol. 56, no. 2, pp. 686–695, Mar. 2007.
[39] R. W. Bauml, R. F. H. Fischer, and J. B. Huber, "Reducing the peak-to-average power ratio of multicarrier modulation by selected mapping," *Electron. Lett.*, vol. 32, no. 22, pp. 2056–2057, Oct. 1996.
[40] A. Alavi, C. Tellambura, and I. Fair, "PAPR reduction of OFDM signals using partial transmit sequence: An optimal approach using sphere decoding," *IEEE Commun. Lett.*, vol. 9, no. 11, pp. 982–984, Nov. 2005.
[41] Y. Zhou, T. Jiang, C. Huag, and S. Cui, "Peak-to-average power ratio reduction for OFDM/OQAM signals via alternative-signal method," *IEEE Trans. Veh. Technol.*, vol. 63, no. 1, pp. 494–499, Jan. 2014.

AIJUN LIU received the B.S. degree in microwave communications, and the M.S. and Ph.D. degrees in communications engineering and information systems from the College of Communications Engineering, Nanjing, China, in 1990, 1994, and 1997, respectively. He is currently a Full Professor with the College of Communications Engineering, PLA University of Science and Technology.

Since 2015, he has been a Visiting Scholar with the Department of Electrical and Computer Engineering, University of Waterloo, Waterloo, ON, Canada. His current research interests include satellite communication system theory, signal processing, space heterogeneous networks, channel coding, and information theory.

SIMING PENG received the B.S. degree in electrical and information engineering from the School of Information Science and Engineering, Wuhan University of Science and Technology, Wuhan, China, in 2012, and the M.S. degree in communications and information system from the College of Communications Engineering, PLA University of Science and Technology, Nanjing, China, in 2015, where he is currently pursuing the Ph.D. degree in communications and information system.

His research interests include satellite communications, signal optimization, and detection.

LI SONG received the B.S. degree in satellite communications, and the M.S. and Ph.D. degrees in communications engineering and information systems from the College of Communications Engineering, Nanjing, China, in 2003, 2006, and 2010, respectively. Her current research interests include satellite communication system theory, signal processing, and modulation and coding.

XIAOHU LIANG received the B.S. degree in communication engineering from the School of Communication and Information Engineering, University of Electronic Science and Technology of China, Chengdu, China, in 2011, and the M.S. and Ph.D. degrees in communications and information system from the College of Communications Engineering, PLA University of Science and Technology, Nanjing, China, in 2013 and 2016, respectively. He is currently a Lecture with the PLA University of Science and Technology.

His research interests include satellite communication, signal processing, and information theory.

KE WANG received the B.S. degree in communication engineering and the M.S. degree in communications and information system from the College of Communications Engineering, PLA University of Science and Technology, Nanjing, China, in 2009 and 2015, respectively, where he is currently pursuing the Ph.D. degree in communications and information system.

His research interests include satellite communication, channel coding, and signal detection.

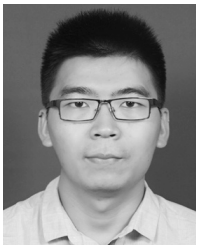

QINGSHUANG ZHANG received the B.S. degree in electronic information science and technology from the School of Electronics Engineering and Computer Science, Peking University, Beijing, China, in 2012, and the M.S. degree in communications and information system from the College of Communications Engineering, PLA University of Science and Technology, Nanjing, in 2014, where he is currently pursuing the Ph.D. degree in communications and information system

His research interests include satellite communication, channel coding, and information theory.